MONTHLY WEATHER REVIEW
VOLUME 96, NUMBER 5
MAY 1968

A NUMERICAL STUDY OF THE DIURNAL VARIATION OF METEOROLOGICAL PARAMETERS IN THE PLANETARY BOUNDARY LAYER

I. DIURNAL VARIATION OF WINDS

K. KRISHNA [1]

National Hurricane Research Laboratory, ESSA, Miami, Fla.

ABSTRACT

The diurnal variation of various meteorological parameters in the Planetary Boundary Layer at different latitudes was studied adopting the basic framework of the simple one dimensional model of Estoque and modifying it in the light of the latest theories of atmospheric turbulence. Following are the results concerning the variation of wind: i) The phase angle of the diurnal wind speed wave shifts with height, the rate of shift varying with latitude. The latter is negative at latitudes north of 30°N., zero at about 30°N., and becomes positive south of 30°N. ii) Low level wind maximum occurs before midnight in midlatitudes, slightly after midnight at 30°N., at sunrise at 17.5°N., and later farther south. iii) The amplitude of the diurnal wind speed wave increases from north to south, reaches a maximum a little below 30°N., and then decreases rapidly. The super-geostrophic winds are strongest between 40°N. and 20°N., suggesting that these latitudes are more favorable for the occurrence of low level jet than any others. The height of the low level wind maximum is below 500 m. north of 30°N., at about 550 m. between 30°N., and 12.5°N. and higher farther south. iv) The winds attain an absolute minimum value by sunrise north of 30°N., and only a relative minimum by about sunset south of 30°N. v) A semidiurnal oscillation of wind speed occurs in the layers below 400 m. north of 30°N., but is not noticed at latitudes south of say 30°N. vi) The Ekman layer appears to be shallower in latitudes south of 30°N. than in more northern latitudes.

1. INTRODUCTION

An improved knowledge of the interaction between the atmosphere and the underlying surface is essential for a satisfactory understanding of the dynamics of the atmosphere and the processes that produce weather. This interaction manifests itself at first in the fluxes of momentum and heat (sensible and latent) and in the profiles of wind, temperature, and humidity in the planetary boundary layer which, in turn, interacts with the free atmosphere. There are several observational and theoretical studies of the behavior of the meteorological parameters in the planetary boundary layer, but our understanding is still far from satisfactory. A theoretical approach to this problem by solving numerically the full set of hydrodynamic equations, making adequate provision for the auto-covariances of the fluctuations, will, no doubt, lead to a better understanding of the behavior of the boundary layer. Estoque [3] has introduced a simple one dimensional model for the study of this layer. That model, modified as discussed below, was used to study the diurnal variation of the various meteorological parameters at different latitudes; for the purposes of comparison, the wind, temperature, and specific humidity in the free atmosphere and the temperature at a specified depth below the soil were kept the same at all latitudes. The results of the study with respect to the variation of wind are presented here.

[1] Permanent affiliation: Institute of Tropical Meteorology, Poona, India. This research was done during 1967 while the author was on a fellowship awarded by the W.M.O.

2. EQUATIONS OF THE MODEL

The equations for the planetary boundary layer, $h \leq z \leq H$, are:

$$\frac{\partial u}{\partial t} = fv - \frac{1}{\rho}\frac{\partial v}{\partial x} + \frac{\partial}{\partial z}\left(K_M \frac{\partial u}{\partial z}\right) \tag{1}$$

$$\frac{\partial v}{\partial t} = -fu - \frac{1}{\rho}\frac{\partial p}{\partial y} + \frac{\partial}{\partial z}\left(K_M \frac{\partial v}{\partial z}\right) \tag{2}$$

$$\frac{\partial \theta}{\partial t} = \frac{\partial}{\partial z}\left(K_H \frac{\partial \theta}{\partial z}\right) \tag{3}$$

$$\frac{\partial q}{\partial t} = \frac{\partial}{\partial z}\left(K_q \frac{\partial q}{\partial z}\right). \tag{4}$$

The equations for the surface boundary layer or constant flux layer, $0 \leq z \leq h$ are:

$$\frac{\partial}{\partial z}\left(K_M \frac{\partial U}{\partial z}\right) = 0 \tag{5}$$

$$\frac{\partial}{\partial z}\left(K_H \frac{\partial \theta}{\partial z}\right) = 0 \tag{6}$$

$$\frac{\partial}{\partial z}\left(K_q \frac{\partial q}{\partial z}\right)=0. \tag{7}$$

The equation for the soil layer, $\zeta_s \leq z \leq 0$ is

$$\frac{\partial T}{\partial t}=K_s \frac{\partial^2 T}{\partial z^2}. \tag{8}$$

U is the magnitude of the wind in the surface boundary layer in which the direction of wind does not change. h is the height of the surface boundary layer, H is the height of the planetary boundary layer, and ζ_s is the depth of soil below which there is no diurnal variation of temperature. The other symbols have their usual meaning. No equality of K_M, K_H, and K_q is assumed.

A term included in Estoque's model to allow for heating due to radiative flux divergence has been omitted from equation (3) above, since the magnitude of such heating during the whole day is of the order of less than 1°C. and is negligible in comparison with heating by solar insolation and turbulent heat fluxes in the layers considered. To simplify the model, horizontal uniformity is assumed and the advection terms have been omitted from equations (1) to (4). The horizontal pressure gradient is assumed constant throughout the layer.

3. PROCEDURES OF THE COMPUTATION

THE GRID

As shown in figure 1, $h=50$ m., $H=2050$ m., and the planetary boundary layer is divided in 20 equal increments of height. Winds, temperatures, and specific humidities are predicted at each of the 19 intermediate levels starting from 150 m. above ground level. The soil layer is divided into 10 equal increments of 5 cm. each. Temperatures are forecast at nine intermediate levels starting from 5 cm. below the surface.

A 5-min. time interval and the explicit finite difference scheme used by Estoque [3] is adopted for integration.

BOUNDARY CONDITIONS

In the soil, at $\zeta_s=50$ cm., the temperature is 294.14°A. At the surface of the earth the no slip condition gives zero wind speed. The temperature of the ground is calculated as discussed at the end of this section. The specific humidity, q, is obtained from saturation mixing ratio at the ground temperature and relative humidity. The ground relative humidity, R, is given by the following empirical function of time,

$$R=59+22\cos\frac{2\pi(t-4)}{24}-11\sin\frac{2\pi(t-4)}{24}$$
$$-3\cos\frac{4\pi(t-4)}{24}+4\sin\frac{4\pi(t-4)}{24}.$$

(R is in percent and t is in hours after midnight.)

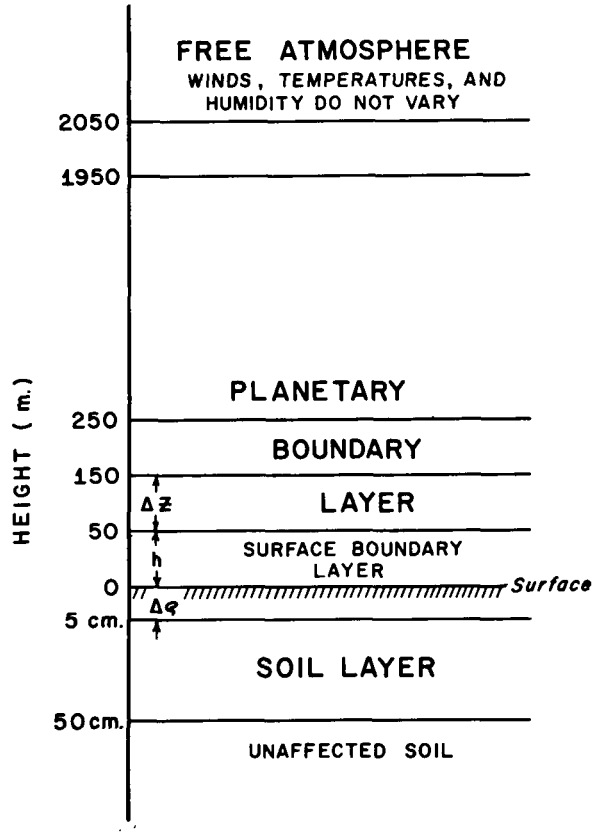

FIGURE 1.—The geometry of the model.

INITIAL CONDITIONS

A realistic set of temperatures and humidities were taken for the grid points in the soil and planetary boundary layer. The initial winds at all grid levels were the assumed geostrophic wind, $u=11$ m./sec. and $v=9$ m./sec.

WIND, TEMPERATURE, AND HUMIDITY PROFILES AND HEAT FLUX

At the interface of the surface and planetary boundary layers, continuity of the gradients of wind, temperature, and humidity is assumed leading to a solution for wind, temperature, and humidity profiles in the surface layer when suitable profile laws of atmospheric turbulence are employed (see Estoque [3]).

In selecting the profile laws Estoque takes into consideration only two regimes of turbulence, viz, free convection and forced convection, separated by a Richardson number of critical value -0.03. Use of this model to cover low latitudes with higher Richardson numbers, R_i, introduced a difficulty. It is known from the literature that the log-linear wind profile formula or its equivalent,

$$\frac{\partial u}{\partial z}=\frac{u_*}{k(z+z_0)}(1+\alpha R_i) \tag{10}$$

cannot hold for extremely stable conditions with large positive values of R_i. When $R_i > -1/\alpha$, we get negative values for u_*. The values for heat flux calculated gradually

decrease before this value of R_i is reached and fall to zero at that value and rise slowly thereafter; see the curve CDE in figure 2. So results obtained in the range of large positive values of R_i are of doubtful validity. Unfortunately, there are no suitable laws of turbulence to cover this range. Possibly there is no turbulence in this range and it is only undulance (see Lumley and Panofsky [6], p. 118). However, for purposes of the model, a critical value of 0.2 for R_i was assumed and the u_* calculated at this value was used for computations of winds, temperatures, humidities, and the fluxes. The curve CFG in figure 2 shows the magnitude of turbulent heat flux calculated between R_i=0.2 and 0.4. A critical value of 0.1 or 0.15 might have been a better choice, but would not have led to materially different results.

Secondly, when R_i decreases below the critical value, the turbulence regime changes from forced to free convection. The finite difference forms for the evaluation of the various parameters, derived from the two different formulations, are different in structure leading to difficulty in ensuring continuity at the critical value. For instance, figure 2 illustrates the discontinuity in turbulent heat flux, which is 25×10^{-4} Ly./min. at point B on the free convection side but 179×10^{-4} Ly./min. at point A on the forced convection side of $R_i = -0.03$. In the finite difference equation for the calculation of heat flux in the free convection regime, the roughness length, z_0, enters as a parameter. It does not appear physically satisfactory to give the same value to it as the length of the roughness elements. A change of its value to 25 cm. instead of 1 cm. ensured continuity of heat flux (see fig. 2). But at the same value, it gave very large values for heat flux at lower Richardson numbers. Moreover, assigning such an arbitrary value to z_0, while computationally expedient, did not appear physically justified.

Recent work by the scientists of Australia (Dyer [1, 2]) has established three important facts, viz:

i) The ratio K_H/K_M, while equal to unity in neutral or near neutral conditions, gradually departs from unity and increases with increasing instability.

ii) From application of similarity theories, the nondimensional wind shear and lapse rate can be expressed as simple functions of the nondimensional height z/L where L is the Monin-Obukhov length,

$$L=-\frac{\rho c_p \bar{\theta} u_*^3}{kgH}.$$

These functions are:

$$\frac{k(z+z_0)}{u_*}\frac{\partial u}{\partial z}=\phi_M\left(\frac{z}{L}\right) \tag{11}$$

$$\phi_M\left(\frac{z}{L}\right)=\left(1-15\frac{z}{L}\right)^{-0.275} \tag{12}$$

$$\frac{k(z+z_0)}{\theta_*}\frac{\partial \theta}{\partial z}=\phi_H\left(\frac{z}{L}\right) \tag{13}$$

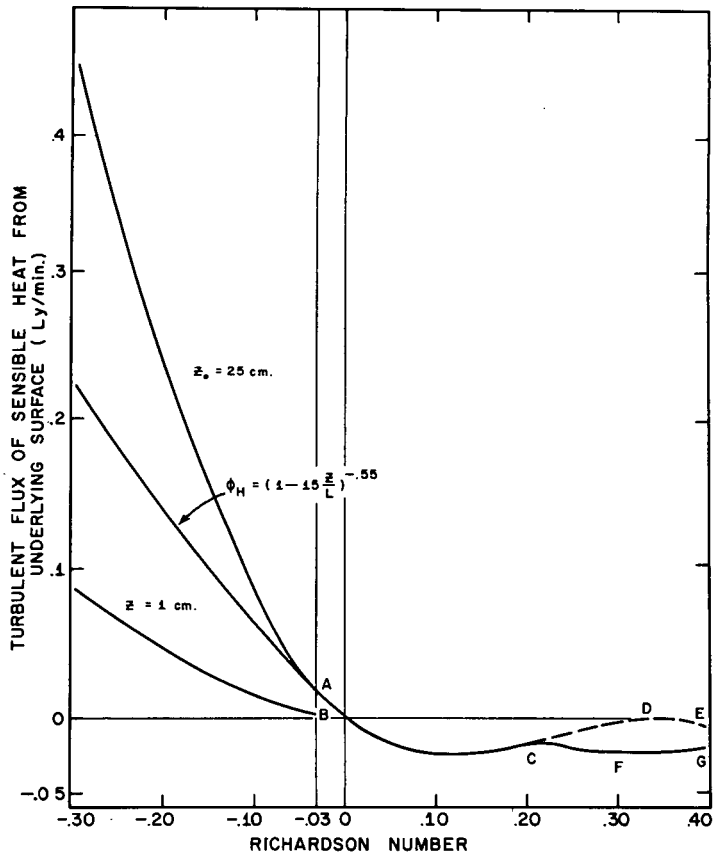

FIGURE 2.—Turbulent flux of sensible heat calculated by different methods.

$$\phi_H\left(\frac{z}{L}\right)=\left(1-15\frac{z}{L}\right)^{-0.55}. \tag{14}$$

iii) The eddy exchange coefficients for latent heat and sensible heat have the same value:

$$\phi_q\left(\frac{z}{L}\right)=\phi_H\left(\frac{z}{L}\right). \tag{15}$$

Here

$$\frac{z}{L}=\frac{K_H}{K_M}R_i. \tag{16}$$

The model makes available a value of R_i computed from winds and temperatures at ground and at the 150-m. level. As a first approximation this value of R_i was assumed to be equal to z/L at level h giving

$$\frac{z}{L}=\frac{R_i}{h}z. \tag{17}$$

Using this equation in equations (11) and (13) and assuming, as stated earlier, continuity of the gradients of wind, temperature, and humidity give

$$u_*=\frac{kU(\Delta z+h)}{\Delta z\cdot\phi_M\left(\frac{h}{L}\right)+\int_0^h \phi_M\left(\frac{z}{L}\right)dz} \tag{18}$$

$$\theta_*=\frac{k(\theta(\Delta z+h)-\theta_0)}{\Delta z\cdot\phi_H\left(\frac{h}{L}\right)+\int_0^h\phi_H\left(\frac{z}{L}\right)dz} \tag{19}$$

$$q_*=\frac{k[q(\Delta z+h)-q_0]}{\Delta z\cdot\phi_q\left(\frac{h}{L}\right)+\int_0^h\phi_q\left(\frac{z}{L}\right)dz} \tag{20}$$

$$H=-\rho c_p u_*\theta_* \tag{21}$$

$$E=-\rho L u_* q_* \tag{22}$$

$$K_M=\frac{ku_*(h+z_0)}{\phi_M(R_i)} \tag{23}$$

$$K_H=\frac{ku_*(h+z_0)}{\phi_H(R_i)} \tag{24}$$

$$K_q=K_H. \tag{25}$$

The above formulation automatically ensures continuity of the variables calculated because, at the critical value of $R_i=0$, we get the logarithmic profiles on either side. See figure 2 for the continuity of the calculations of the flux of sensible heat.

Table 1 gives an illustration of the computed values of R_i, K_M, K_H, and K_H/K_M at selected latitudes at 1 p.m. local time, when these parameters take extreme values.

Values of K_H/K_M falling between 1.58 and 1.93 appear reasonable in the light of the latest computations of this ratio.

GROUND TEMPERATURE

The temperature at the ground is obtained by solving for that temperature which balances the sum of

F_1, upward long wave radiation,
F_2, downward long wave radiation,
F_3, turbulent heat flux,
F_4, heat flux into the soil, and
F_5, the short wave radiation received from the sun.

These fluxes are evaluated from the formulae

$$F_1=\sigma T^4 \tag{26}$$

$$F_2=4083\times10^{-6}-1.195\sigma T^4 \tag{27}$$

$$F_3=-\rho\left(c_p K_H\frac{\partial\theta}{\partial z}+LK_q\frac{\partial q}{\partial z}\right) \tag{28}$$

TABLE 1.—*Values of R_i, K_M, K_H, and K_H/K_M at 1 p.m. local time*

	Latitude (°N.)				
	55.0	42.5	30.0	17.5	7.5
R_i	−0.28	−0.37	−0.67	−0.51	−0.52
K_M ($m.^2/sec.$)	14.78	15.22	14.72	15.28	15.12
K_H ($m.^2/sec.$)	23.28	25.32	28.46	27.65	27.51
K_H/K_M	1.58	1.66	1.93	1.81	1.82

$$F_4=-\rho_s C_s K_s\frac{\partial T}{\partial z} \tag{29}$$

$$F_5=-\mu I(\sin\phi\sin\delta+\cos\phi\cos\delta\cos\psi) \tag{30}$$

where μ is combined albedo and turbidity factor and I is the solar constant. The other symbols have their usual meaning. The value assumed for μ is 0.9 and for I, 2 Ly./min.

The value of F_2 is obtained from an empirical formula by Swinbank [8] for the computation of downward long wave radiation. The ground temperature was taken as equivalent to the temperature of the air near the ground. This formula, which claims a correlation of 0.998 between computed and observed values, is a considerable simplification over elaborate calculations made by using a radiation formula that calls for the computation of optical depths, emissivity gradients, and integration. Use of Swinbank's formula saves considerable time without compromising accuracy.

4. RESULTS OF THE INVESTIGATION

The numerical model described above was integrated for 5 days. After the first day the contours of wind, temperature, and humidity attain a uniform diurnal pattern, with little or no difference from 1 day to another. It was therefore decided to adopt the results of the third day as representing the equilibrium state of diurnal variation. Integrations made at 12 latitudes between 55°N. and 2.5°N. were used in this study. The diurnal variation of wind speed has been analyzed and presented below with available supporting observational evidence.

SHIFT OF TIME OF MAXIMUM (MINIMUM) WITH HEIGHT

Figure 3 shows, for selected latitudes, isotachs on a height vs. time chart reproduced from the computer output. It may be noted that the winds at 2 km. are the same at all latitudes facilitating a comparison between latitudes. The isotachs exhibit a characteristic tilt which changes with latitude. At 30°N. and 26°N. the isotachs have little or no tilt to the right or left. This means that the maximum or minimum of diurnal oscillations occurs at the same time at all heights above the ground at those latitudes. North of 30°N. the isotachs are inclined to the left, the inclination increasing with latitude, implying that the maximum (minimum) of diurnal oscillation of wind occurs earlier as one reaches higher altitudes. In other words, there is a retardation with height of the phase angle of the diurnal wave, the rate of retardation increasing north of 30°N. South of 30°N., however, the isotachs incline to the right, implying that the maxima at these latitudes occur later in the day as one reaches higher altitudes; i.e., there is an increase with height of the phase angle of the diurnal wave. This increase reaches a maximum and then falls as one approaches the Equator.

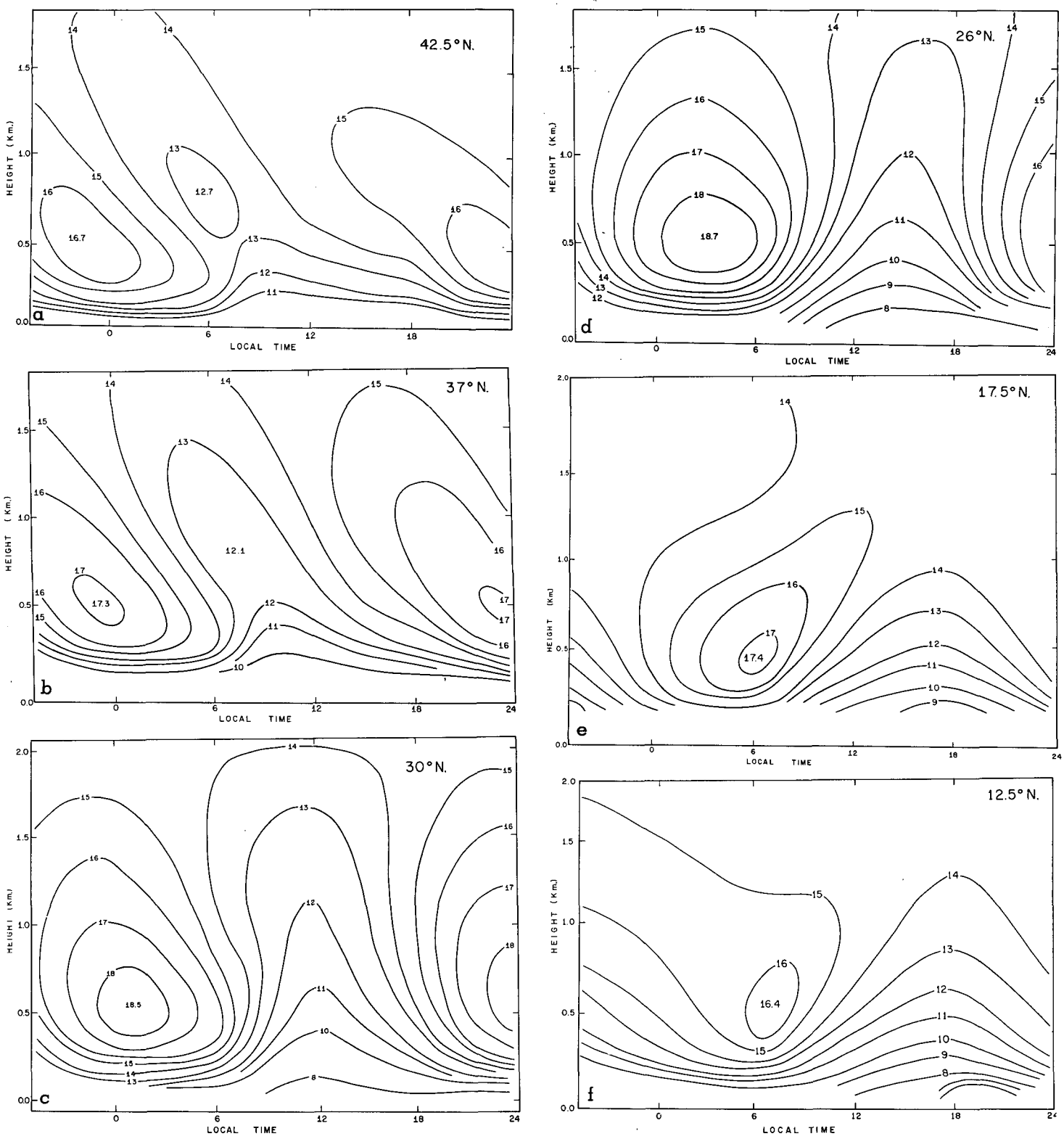

FIGURE 3.—Computed diurnal variation of wind speed in m./sec. (figures inside the closed isotachs are extreme values reached) at (a) 42.5°N., (b) 37°N., (c) 30°N., (d) 26°N., (e) 17.5°N., and (f) 12.5°N.

Table 2 gives the computed magnitudes and time and height of occurrence of the maximum (minimum) wind speed and also the average tilt of the phase angle of the diurnal wave at various latitudes. Figure 4 shows the observed isotachs over O'Neill, Nebr., on Aug. 24–25, 1953. These observations were given by Lettau and Davidson [5]. Figure 5 provides evidence for less rapid rate of retardation of phase angle at 37°N. and figure 6,

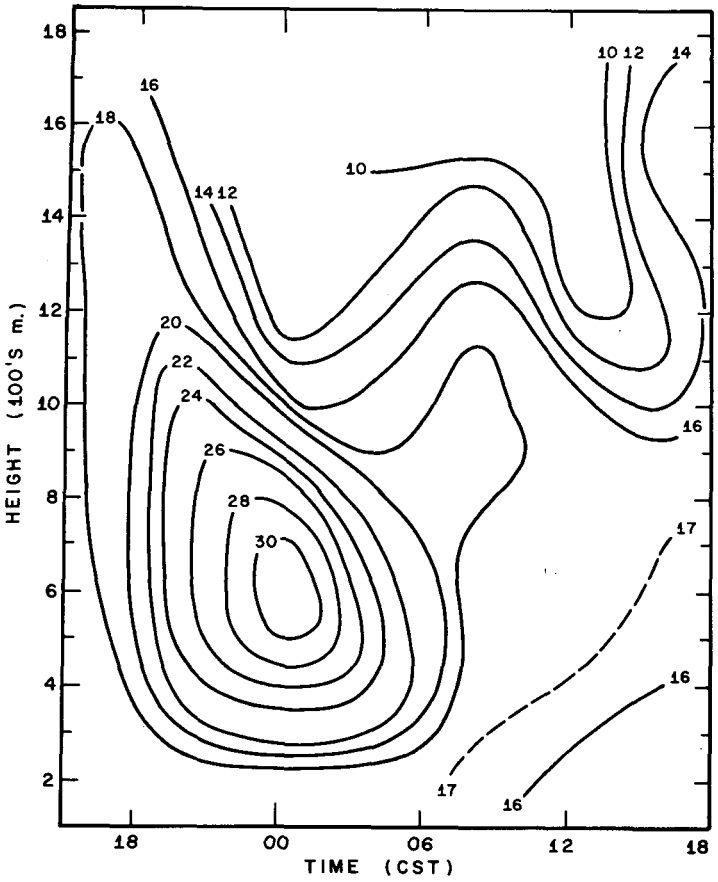

FIGURE 4.—Observed diurnal variation of wind speed in knots over O'Neill, Nebr. (42.5°N.), on Aug. 24–25, 1953 (data taken from Lettau and Davidson [5]). Average rate of retardation, with height of the phase angle of diurnal wind speed wave, observed: 8 hr./km.; calculated: 9 hr./km.

TABLE 2.—*Magnitudes and time and height of occurrence of low level wind speed maximum and minimum and the average tilt of the axis of the maximum*

Latitude (°N.)	Maximum			Minimum			Average tilt of the axis of the maximum (hr./km.)
	Speed (m./sec.)	Time (LST)	Height (m.)	Speed (m./sec.)	Time (LST)	Height (m.)	
55.0	16.4	22	450	13.0	05	650	−10
50.0	16.5	23	450	13.0	06	650	−8
42.5	16.7	23	450	12.7	06	750	−8
37.0	17.1	23	450	12.0	07	850	−6
30.0	18.5	01	550	----------	----------	----------	−2
26.0	18.8	03	550	----------	----------	----------	0
17.5	17.4	06	450	----------	----------	----------	6
12.5	16.4	07	550	----------	----------	----------	4
10.0	16.6	08	750	----------	----------	----------	4
7.5	16.4	09	1050	----------	----------	----------	3
5.0	15.0	11	1350	----------	----------	----------	----------

for in-phase waves at all heights over 26°N. The agreement between observed and computed values of the rate of change of the phase angle with height is remarkable.

TIME OF OCCURRENCE OF LOW LEVEL WIND MAXIMA

The low level wind maxima do not occur at the same time of the day at all latitudes (see figs. 3 and 7a). The occurrence of the wind maximum about midnight in the midlatitudes is well known. The numerical computations show that under the effect of the curvature of the earth

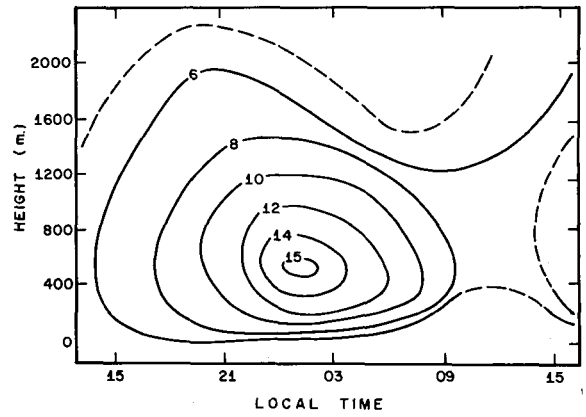

FIGURE 5.—Observed diurnal variation of average wind speed in m./sec. over Wichita and Oklahoma City (37°N. mean latitude) during a 24-day period. Average rate of retardation, with height, of the phase angle of diurnal wind speed wave, observed: 4 hr./km.; calculated: 6 hr./km. (Data supplied by Prof. A. K. Blackadar.)

TABLE 3.—*Morning and midday wind speeds (mi./hr.) over Khartoum, Sudan (15.6°N.)*

Height (m.)	150	300	600	900	1200	1500
Jan. a.m.	24	33	28	17	9	9
p.m.	10	13	15	14	9	7
Apr. a.m.	14	17	20	19	15	12
p.m.	12	10	10	10	7	5
July a.m.	15	20	22	18	11	7
p.m.	12	11	15	16	12	9
Oct. a.m.	4	3	6	13	13	11
p.m.	4	4	5	6	9	12

and its rotation alone, the time of occurrence of the maximum changes with latitude. It comes before midnight at 55°N., gradually approaches midnight as one approaches 30°N., but recedes rapidly as one goes south, coming at sunrise near 17°N. and after sunrise at more southern latitudes. The observations of winds over Gwalior (26°N.), where the maximum occurs between midnight and sunrise, provide partial evidence for the above features.

Farquharson [4] found that upper winds over Khartoum (15.6°N.) decrease from morning to midday and that "the diurnal variation observed extends over a belt of latitude from 20°N. to 20°S." Table 3 gives an extract from the observations quoted in that paper. Based on upper air observations over Khartoum, a suggestion was made by Farquharson that the observed phenomenon was due to a fall in geostrophic wind from morning to midday, brought about by a diurnal variation of the temperature gradient. The arguments for such a variation of temperature gradient are complicated and are not claimed to be well established. While not repudiating this hypothesis, it is suggested, on the basis of computations shown in figures 3e and 3f that even without any temperature gradient the rotation of the earth alone is sufficient to account for a fall of wind speed from the morning to midday at the latitudes in question. It is significant to note that the above phenomenon is said

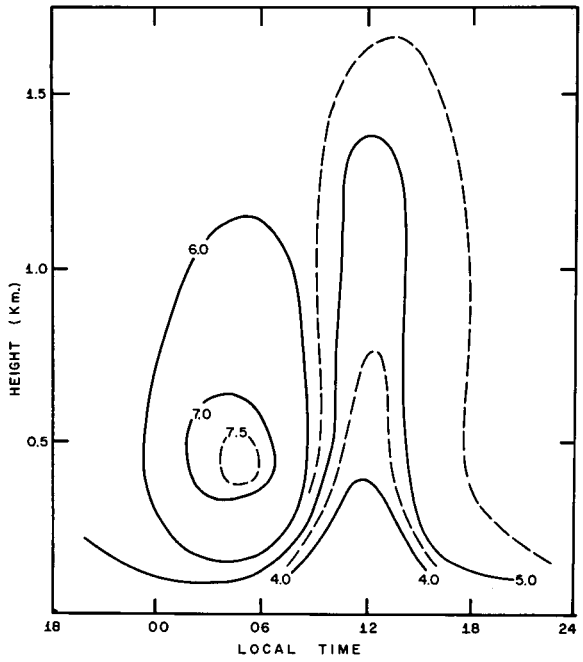

FIGURE 6.—Observed diurnal variation of wind speed in m./sec. over Gwalior, India (26°N.), during April 1962. Average rate of retardation, with height, of the phase angle of diurnal wind speed wave, observed and calculated: 0 hr./km. (Data collected from the records of India Meteorological Department.)

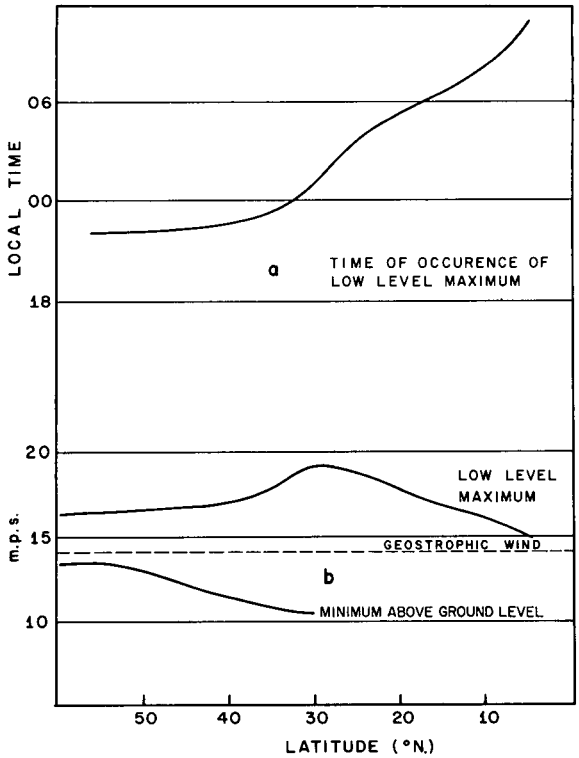

FIGURE 7.—(a) Time of occurrence of maximum wind speed at different latitudes. (b) Maximum and minimum wind speeds at different latitudes.

to occur at several places over the entire African Continent between 20°N. and 20°S. It may not be a coincidence that the difference between morning and midday wind speeds over Khartoum is highest at 300 m. and 600 m.; for the wind maximum at latitude 17.5°N. is reached at a level of 450 m. at the time of sunrise (see fig. 3e). It will be interesting to test all the implications of the prediction of the numerical solution shown in figure 3e with wind observations over Khartoum or any other continental African station, taken at intervals of 6 or fewer hr., if such are available.

MAGNITUDE OF SUPER-GEOSTROPHIC WINDS

Figure 7b shows the maximum wind speeds in the low levels at different latitudes are super-geostrophic. The departure from the geostrophic speed increases gradually as one reaches southern latitudes, attains a maximum at 30°N., and then falls faster till the maximum attains nearly geostrophic values nearer the Equator. This figure shows that the effect of the earth's curvature alone accounts for a considerable contribution to the low level wind maximum. It also suggests that the latitudes between 40°N. to 20°N. are more favored for low level jet phenomena than latitudes north or south of it.

Table 2 also shows that the height of occurrence of the wind maxima is at about 450 m. north of 30°N., about 550 m. between 30°N. and 12.5°N., and higher farther south.

MINIMUM WINDS AT LEVELS ABOVE THE SURFACE

North of 30°N. (see fig. 3a and 3b), about the time of sunrise, the vertical profile of wind speed exhibits an absolute minimum value near 700 m. This means that, during that period, as one goes from the ground to higher levels, the wind speeds reach a maximum, then a minimum, and again rise to the geostrophic value. Such a minimum does not occur at 30°N. and farther south (see also fig. 7b). In these southern latitudes relative minima at each level occur practically in phase at all levels about sundown.

SEMIDIURNAL OSCILLATION OF WINDS BELOW 400 M.

The prediction of semidiurnal oscillation by the model was noted earlier by Estoque [3]. Figure 8, which shows the isotachs of computed winds plotted on a chart of logarithm of height vs. time, focuses attention on wind variation at levels below 400 m. At 50°N. lat. there is a well-marked semidiurnal oscillation of wind, with maxima in the afternoon and before midnight, and minima before sunrise and after sunset. This provides a theoretical explanation of the semidiurnal oscillation of wind that has long been known from the literature on the subject. References to it are also contained in standard meteorological text books. Recently Singer and Raynor [7] have analyzed the winds over Brookhaven and brought out the details of this phenomenon at that station (see fig. 9). The similarity between figure 9 and figure 8a, the computed winds for 50°N., is noteworthy.

Computations for 30°N. (fig. 8b) show that here the picture is different. Minima occur at midday and late evening and maxima occur after sunrise and before sunset.

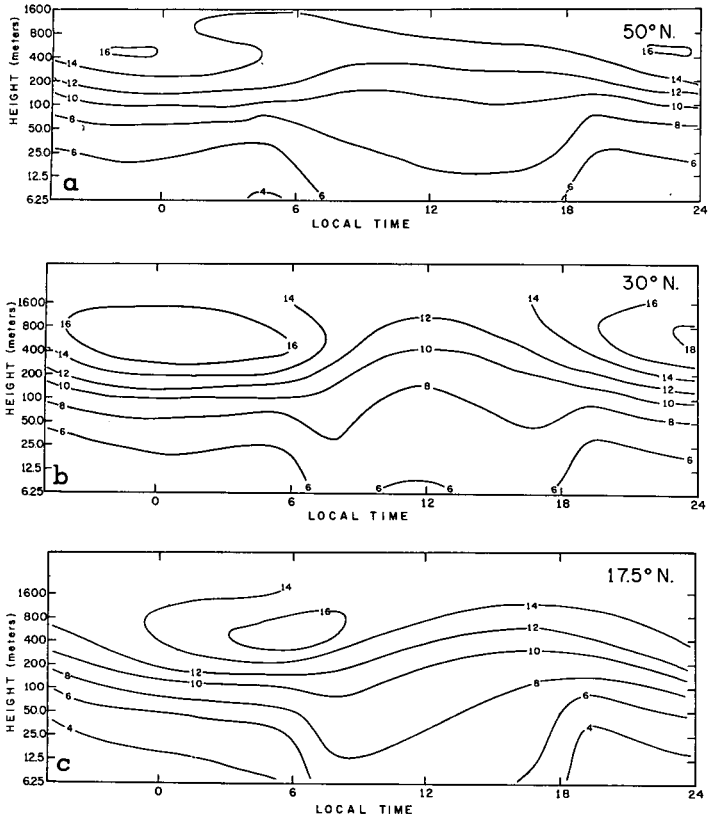

FIGURE 8.—Computed diurnal variation of wind speeds in m./sec. at lower levels at three typical latitudes: (a) 50°N., (b) 30°N., and (c) 17.5°N. Note the semidiurnal oscillation and the position of the day maximum at different levels.

Farther south no semidiurnal oscillation is noticeable. At 17.5°N., the maximum winds at all levels occur in the morning. The observations over Khartoum (see table 3) can be cited as evidence for this.

DEPTH OF THE EKMAN LAYER

The height at which the wind maximum occurs increases as one goes from 30°N. towards the Equator (see table 2). But the layer, where the wind speed departs by more than say 1 m./sec. from the geostrophic wind speed, becomes increasingly shallower (see fig. 3e and f). Since the earth's rotation is responsible for much of the wind variation above 400 m., the variations can be expected to be smaller nearer the Equator where the effect of the earth's rotation is smaller.

The results presented here do not take into consideration the vertical variation of pressure gradients in the planetary boundary layer and the advection of heat and momentum, which may to some extent vary the isotach patterns. It is proposed to study such variations at a later stage of the investigation undertaken here.

Any phenomenon depending upon solar insolation, which has sinuous variation during the day and zero variation during night, is rich in harmonics. Besides the periodicity of solar insolation which affects winds in the boundary layer through its effect on eddy exchange coefficients, the period of the pendulum day has also its own influence. The effect noticed here is, presumably, a result of the interaction between these two periods.

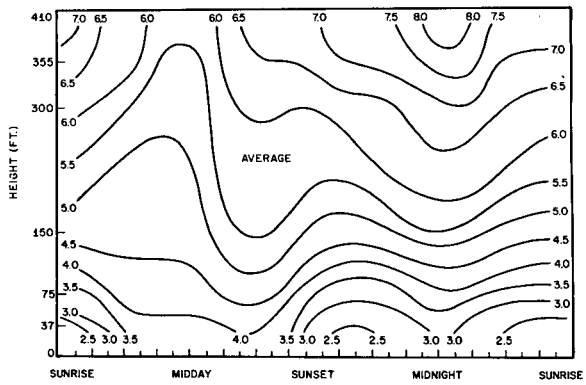

FIGURE 9.—Observed diurnal variation of wind speed over Brookhaven National Laboratory, after Singer and Raynor [7].

ACKNOWLEDGMENTS

I am grateful to the World Meteorological Organization and to the Government of India for giving me a fellowship and opportunity to undertake this research work. I am thankful to the Environmental Science Services Administration for affording facilities to work at several of its research establishments and especially for making expensive computer time liberally available, and to the various ESSA scientists for ungrudgingly giving their time for discussion.

I am also thankful to Dr. Takashi Nitta of Japan Meteorological Agency for initiating me in this research project, to Dr. A. J. Dyer for supplying me the latest results of the C.S.I.R.O. regarding the analytic form of the ϕ-function, to Prof. A. K. Blackadar for supplying the Wichita observations, to the Director General of Observatories, India, for the Gwalior observations, and to Prof. Estoque for the valuable discussions I had with him.

REFERENCES

1. A. J. Dyer, "The Turbulent Transport of Heat and Water Vapour in an Unstable Atmosphere," *Quarterly Journal of the Royal Meteorological Society*, vol. 93, No. 398, Oct. 1967, pp. 501–508.
2. A. J. Dyer, personal communication, 1967.
3. M. A. Estoque, "A Numerical Model of the Atmospheric Boundary Layer," *Journal of Geophysical Research*, vol. 68, No. 3, Feb. 1963, pp. 1103–1113.
4. J. S. Farquharson, "The Diurnal Variation of Wind Over Tropical Africa," *Quarterly Journal of the Royal Meteorological Society*, vol. 65, 1939, pp. 165–183.
5. H. H. Lettau and B. Davidson, *Exploring the Atmosphere's First Mile*, Pergamon Press, New York, 2d vol., 1957, 578 pp.
6. J. L. Lumley and H. A. Panofsky, *The Structure of Atmospheric Turbulence*, Interscience Publishers, New York, 1964, 239 pp.
7. I. A. Singer and G. S. Raynor, "A Solar Time Classification for Meteorological Use," *Bulletin of the American Meteorological Society*, vol. 39, No. 11, Nov. 1958, pp. 569–573.
8. W. C. Swinbank, "Long-Wave Radiation From Clear Skies," *Quarterly Journal of the Royal Meteorological Society*, vol. 89, No. 381, July 1963, pp. 339–348.

[*Received September 26, 1967; revised November 27, 1967*]